Thin–Walled Structures 192 (2023) 111138

Contents lists available at ScienceDirect

Thin-Walled Structures

journal homepage: www.elsevier.com/locate/tws

Full length article

Guided wave-based characterisation of cracks in pipes utilising approximate Bayesian computation

Zijie Zeng, Min Gao, Ching Tai Ng *, Abdul Hamid Sheikh

School of Architecture and Civil Engineering, The University of Adelaide, Adelaide, SA 5005, Australia

ARTICLE INFO

Keywords:
Damage identification
Pipe
Bayesian approach
Approximate Bayesian computation
Spectral finite element
Guided waves
Torsional wave

ABSTRACT

This paper proposed a probabilistic framework of damage characterisation to detect and identify early-state cracks in pipe-like structures using ultrasonic guided waves. The crack location, crack sizes (e.g., depth and width of the crack), and Young's modulus are considered as unknown parameters in the model updating using a Bayesian approach, by which their values and the associated uncertainties are quantified. The proposed framework is developed based on approximate Bayesian computation (ABC) by subset simulation, which is a likelihood-free Bayesian approach. This algorithm estimates the posterior distributions of unknown parameters by directly accessing the similarity between the measured signals from experiments and the simulated guided wave (GW) signals from the numerical model. In this case, the evaluation of likelihood functions can be smartly circumvented during Bayesian inference. A time-domain spectral finite element (SFE) method with a cracked finite element model is employed to model the pipes to enhance the computational efficiency of the simulation and model updating. Numerical and experimental case studies are carried out to evaluate the performance of the proposed likelihood-free approach. Numerical results show the accuracy and robustness of the proposed approach in identifying unknown parameters under different scenarios. The associated uncertainties of each parameter are also quantified by analysing the statistical properties of the sample set, such as mean and coefficient of variation (COV) values. Experimental results show that the proposed method can accurately identify the unknown parameters, which further verifies the accuracy and practicability of the probabilistic damage characterisation framework.

1. Introduction

1.1. Structural health monitoring

Damage detection is considered as one of the main components in structural health monitoring (SHM). Adequate and regular health inspection of structural integrity is essential to the safety, serviceability, and reliability of structures. Numerous sophisticated non-destructive testing (NDT) techniques were developed with the advancement of computers and sensors over the past few decades [1]. These techniques are generally typified by simple visual inspection, conventional A- or C-scan ultrasonic testing, eddy current, acoustic emission, vibration-based approaches utilising low-frequency vibration testing [2] and guided wave (GW) based approaches [3].

The vibration-based techniques are efficient in global monitoring by utilising modal parameters or dynamic responses of structures. However, some studies reported that they are insensitive to minor local defects, which may still be critical to the structural safety [4]. On the other hand, guided wave-based techniques have been proven to be sensitive in detecting various types of local defects because of the wave propagation characteristics of high-frequency waves and the waves have long propagation distance [5]. GW propagating in structures is commonly classified into one-dimensional (1D) waveguides and two-dimensional (2D) waveguides. Pipes and beams are some typical examples of 1D waveguides [6,7], while examples of 2D waveguides are shells and plates [8,9].

1.2. Guided wave based techniques in pipe-like structures

Pipes-like structures have extensive applications in industries (e.g., chemical and oil industries) and in our daily life (e.g., water pipeline systems). Common defects in such thin-walled and hollow-cylindrical structures are pits, blockages, and corrosion [10–14]. Incipient defects in pipes, even a single crack, can lead to severe consequences and even

* Corresponding author.
E-mail address: alex.ng@adelaide.edu.au (C.T. Ng).

https://doi.org/10.1016/j.tws.2023.111138
Received 18 April 2023; Received in revised form 27 June 2023; Accepted 24 August 2023
Available online 29 August 2023

catastrophic failures or accidents without timely inspection and manual intervention. Guided wave based techniques have attracted much attention because the multimode-guided waves can propagate in both circumferential and axial directions of the pipe over a long distance [15]. GW presents the potential capacity to detect various flaws on the outside and inside surfaces of pipes in inaccessible areas.

GW modes in circular waveguide can be named as $T(0,n)$, $L(0,n)$ and $F(m,n)$, standing for torsional, longitudinal, and flexural modes, where m and n denotes the circumferential order and group order of the wave modes, respectively [15]. Each mode has its unique wave characteristics, and the choice of wave mode mainly depends on the targeted damage type and the specific detection requirement. Axisymmetric wave modes, including longitudinal and torsional modes, are generally preferable because they are easier to be generated [6]. In particular, the fundamental torsional $T(0,1)$ mode has demonstrated significant practicability in damage assessment recently because of its insensitivity to the presence of fluid and insulation materials, as well as its non-dispersive wave characteristic over the whole frequency range. Besides, no other torsional wave modes will be excited if the excitation frequency is below the cut-off frequency of $T(0,2)$ [6,15–17]. In the literature, some studies investigated the torsional waves propagation in pipes and the scattering phenomenon due to cracks. For instance, Løvstad and Cawley investigated the torsional wave reflection phenomenon from multiple circular flaws in pipes [18]. Kwun et al. experimentally investigated the attenuation of the fundamental torsional waves in a coal-tar-coated pipe above ground and underground [19]. A quantitative study regarding the fundamental torsional wave reflection from axisymmetric and non-axisymmetric cracks in pipes was conducted using finite element simulations and further validated by conducting experimental studies [16]. Huan et al. measured the attenuation of the $T(0,1)$ mode in embedded pipes with different coating materials [20]. The studies mentioned above generally detect damage by examining linear feature changes (e.g., time of flight, mode conversion, and attenuation) in wave scattering induced by the interaction of incident waves and structural damage. Although some studies have investigated the GW based approaches for detecting cracks in pipes using torsional waves, there is still significant room for further exploring the quantification of damage characteristics, especially using an advanced model based approach.

Various GW model based methods have been proposed to characterise different types of defects in different types of structures [21,22]. Specifically, an analytical or numerical model is employed to describe the propagation of guided waves and the scattering at cracks. The crack characteristics of location and severity (e.g., width and depth) are considered unknown parameters in the model for updating. The damage quantification is conducted by optimising the crack parameters of the numerical model, in which the differences between the numerical guided wave signals and measured ones are minimised. GW model based approach can provide extra quantitative information on the damage detection [23,24]. Hence, this paper proposes a GW model based approach for crack characterisation in pipe-like structures.

1.3. Bayesian probabilistic framework

To enhance the reliability and robustness of structural damage characterisation, uncertainties in both numerical simulation and experimental observation, such as modelling simplification, measurement error due to environmental noise and systematic error, as well as manufacturing and material variability, should be appropriately considered [25–27]. amongst the approaches for damage identification under uncertainty in engineering structures, the Bayesian statistical framework is one of the well-established approaches, which explicitly considers the uncertainty quantification in the procedure of damage characterisation by employing the Bayesian inference. Various Bayesian methods and illustrated examples can be found in the literature [27–29].

The Bayesian approach has been considered in GW based damage identification. For example, Ng and his coworkers employed a Bayesian statistical framework in isotropic and composite beam structures to identify single and multiple cracks with associated uncertainty quantification by incorporating different signal processing techniques and a spectral finite element (SFE) method [23,24]. Yan utilised the information on the time-of-flight in the scattered lamb wave to characterise the unknown crack location and wave velocity parameters in beams [30]. Cantero-Chinchilla et al. proposed a multilevel Bayesian framework using hybrid wave finite element (WFE) methods to classify, localise, and quantify damages in composite beam structures from the completed measured time-domain ultrasound signals [31]. Yan et al. proposed a Bayesian damage identification framework based on an analytical probabilistic model and an ultrafast wave scattering simulation scheme [32]. Most of the studies focused on Bayesian damage identification using guided wave generally focused on beams and plates, while very limited applications were conducted in pipe-like structures [33].

In Bayesian inference, the prior is often a non-informative distribution, which tends to be determined by the user experience, and hence, the likelihood function is the key component to estimate the posterior. Nevertheless, situations can always happen whereby the model or problem is so complex that the full analytical likelihood function might be computationally expensive to evaluate or even intractable [34,35]. In addition, the selection of the likelihood function is related to the assumptions of error between observation and model made on the underlying unknown data-generating distribution. Different forms of likelihood function might lead to different subsequent posterior distributions. In other words, no universal form of the likelihood can be used in any circumstances [34,35].

To make the Bayesian probabilistic framework for GW based damage detection more practical, a likelihood-free approach, approximate Bayesian computation (ABC), is employed as a more feasible and straightforward algorithm. ABC provides an alternative to solving the inverse problem that directly accesses the similarity between simulation and measurement using a distance function to identify the unknown posterior distribution without requiring explicit likelihood function evaluation [34,35]. Thereby, the difficulty of the likelihood function mentioned above is smartly overcome. It should be noted that the selection of distance functions is one of the key concerns in ABC algorithms. An inappropriate selection could impact inference accuracy and even introduce additional bias in estimation [35]. Final tolerance level selection is also crucial to simulation performance. A too-small threshold tends to require more simulation time, while a too-large value may lead to inaccurate prediction. In other words, there is always a trade-off between efficiency and accuracy in tolerance level selection [36]. During the last decades, much effort has been devoted to overcoming these difficulties and improving ABC performance in both efficiency and accuracy. The reader can refer to the comprehensive review in the literature [34–37]. Numerous variants of ABC have been successfully employed in vibration-based approaches for parameter estimation and model selection [38,39]. Chiachio et al. [40] combined the ABC framework into the subset simulation techniques [41,42] to estimate rare-event, and it has demonstrated good computational efficiency as well as the same or better precision as other ABC algorithms, such as ABC Markov chain Monte Carlo (MCMC) [43] and ABC sequential Monte Carlo (SMC) [44]. Recently, Fakih et al. proposed a Bayesian probabilistic framework for damage characterisation in welded structures using Lamb-wave surrogate models training from Artificial Neural Network (ANN) and minimal sensing, incorporating an approximate Bayesian computation framework [45].

To summarise, torsional waves have been shown to be effective in detecting damage to pipe-like structures. It is worthwhile evaluating a procedure for locating the damage and also identifying the corresponding properties. GW model based approaches have been proposed for damage characterisation by minimising the discrepancy between simulation and measurement. In particular, Bayesian approaches have

been commonly incorporated into the model based framework, which can explicitly take uncertainty quantification into account. Most Bayesian GW damage identification frameworks were established depending on different likelihood function assumptions. To make the framework more practical, ABC provides an alternative way to solve the inverse problem with the Bayesian approach. In this study, a likelihood-free probabilistic framework for damage characterisation in pipe-like structures using torsional guided waves is proposed. The likelihood-free probabilistic framework is developed based on approximate Bayesian computation by subset simulation (ABC_SubSim) to overcome the aforementioned challenges in evaluating the likelihood function. A time-domain SFE model is used to simulate the numerical signals of torsional guided wave propagation and the phenomenon of scattering in pipes. The time-domain SFE and the conventional finite element (FE) method have the same flexibility in model discretisation, while SFE method provides a more effective tool in GW propagation simulation by using high-order approximation polynomials that require fewer finite elements in model construction. A spectral crack element is embedded in SFE model to simulate the crack and also consider the effect of the torsional-flexural mode conversion due to the interaction of the GW propagation with the cracks [46]. The unknown parameters, such as crack location, crack size, and other material properties, and their associated uncertainties, can be quantified by minimising the discrepancy between the numerical and measured guided wave signals.

The arrangement of the paper is listed below. Section 2 presents the details of time-domain SFE method of pipe, incorporating a spectral cracked element. The algorithm of ABC-SubSim is presented in Section 3. In Section 4, numerical studies are conducted to investigate the robustness and accuracy of the proposed framework. Experimental studies are also carried out to further verify the accuracy and practicability of the likelihood-free framework. Finally, conclusions are drawn in Section 5.

2. Time-domain spectral finite formulation of torsional guided wave in pipes

2.1. Timoshenko beam theory and elementary rod theory

The numerical model for the pipe is developed using the time-domain SFE method based on Timoshenko beam theory and elementary rod theory [47]. The elementary rod theory governs the torsional wave motion about u-axis, θ, based on the principle of Saint-Venant. The vertical displacement along v-axis, v, and the effect of shear deformation about w-axis, φ, are considered by the Timoshenko beam theory. Thus, three degrees-of-freedom (DoFs) were considered in the simulation of the pipe element, as shown in Fig.1.

The governing equations are defined as [48,49]

$$GJ\frac{\partial^2\theta}{\partial x^2} + F_\theta(x,t) = \rho I_o\ddot{\theta} \tag{1}$$

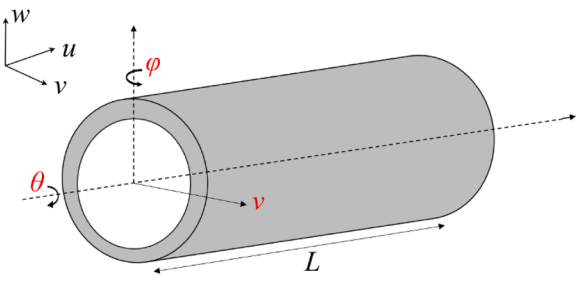

Fig. 1. Spectral finite element with length L for the fundamental torsional wave.

$$K_1^{Tim}GA\frac{\partial}{\partial x}\left(\frac{\partial v}{\partial x} - \varphi\right) = \rho A\ddot{v} - F_V(x,t) \tag{2}$$

$$EI\frac{\partial^2\varphi}{\partial x^2} + K_1^{Tim}GA\left(\frac{\partial v}{\partial x} - \varphi\right) = K_2^{Tim}\rho I\ddot{\varphi} \tag{3}$$

where A, J, ρ, E and G is the cross-section area, the polar moment of inertia, material mass density, Young's modulus, and shear modulus, respectively. I and I_o is the second moment of inertia about w-axis and u-axis, respectively. The external vertical and torsional excitation are represented by $F_V(x,t)$ and $F_\theta(x,t)$. The parameters K_1^{Tim} and K_2^{Tim} are adjustable factors introduced in Timoshenko beam theory for the fact that the actual distributed shear strain is not constant as assumed [48]. In this paper, $K_1^{Tim} = 0.28$ is defined from the experimental results of the pipe model (described in Section 5), by which the SFE numerical simulation has the best fit to the measurement. $K_2^{Tim} = 45K_1^{Tim}/\pi^2$ is applied to match the cut-off frequency of GW modes [48,49].

2.2. Time-domain spectral finite element method

In the time-domain SFE method, the GW propagation simulation can be expressed by an ordinary differential equation:

$$\mathbf{M}\ddot{\mathbf{U}} + \mathbf{C}\dot{\mathbf{U}} + \mathbf{K}\mathbf{U} = \mathbf{F}(t) \tag{4}$$

where the displacement, velocity, and acceleration are denoted by $\mathbf{U}$, $\dot{\mathbf{U}}$ and $\ddot{\mathbf{U}}$. **M, C** and **K** is the global mass matrix, global damping matrix, global stiffness matrix and the global load vector are illustrated by $\mathbf{F}(t)$, respectively. **C** is dependant on $\boldsymbol{M}$ with the relationship $\boldsymbol{C} = \eta\boldsymbol{M}$, where η is the damping coefficient [50].

$\mathbf{M}^e$, $\mathbf{K}^e$ and $\mathbf{F}^e$ is the element mass matrix, element stiffness matrix and the element load vector, respectively. The expressions are presented as follows:

$$\mathbf{M}^e \approx \sum_{i=1}^{n} \mathrm{w_i}\mathbf{N_e}(\xi_\mathrm{i})^\mathrm{T}\boldsymbol{\mu}\mathbf{N_e}(\xi_\mathrm{i})\det(\mathrm{J}^e(\xi_\mathrm{i})) \tag{5}$$

$$\mathbf{K}^e \approx \sum_{i=1}^{n} \mathrm{w_i}\mathbf{B_e}(\xi_\mathrm{i})^\mathrm{T}\mathbf{D}\mathbf{B_e}(\xi_\mathrm{i})\det(\mathrm{J}^e(\xi_\mathrm{i})) \tag{6}$$

$$\mathbf{F}^e \approx \sum_{i=1}^{n} \mathrm{w_i}\mathbf{N_e}(\xi_\mathrm{i})^\mathrm{T}\mathbf{f}(\xi_\mathrm{i})\det(\mathrm{J}^e(\xi_\mathrm{i})) \tag{7}$$

where n is the number of Gauss-Lobatto-Legendre (GLL) nodes at each spectral element. $\mathbf{f}(\xi_\mathrm{i})$ is the external excitation. **D** and **μ** is the stress-strain matrix and the mass density matrix. $\mathrm{J}^e = \frac{\partial x}{\partial \xi}$ is the Jacobian function used for coordinate transformation from the local matrix to the global matrix [51].

ξ_i is the local coordinate of the GLL point with domain from −1 to 1, which can be calculated by the following equation:

$$\left(1-\xi_i^2\right)\frac{dL_{n-1}(\xi_i)}{d\xi_i} = 0 \text{ for } i \in 1,\ldots,n \tag{8}$$

where L_{n-1} is the first derivative of Legendre polynomial of degree (n-1). The weight function w_i of the corresponding GLL node ξ_i are determined as

$$w_i = \frac{2}{n(n-1)\left(L_{n-1}(\xi_i)\right)^2} \text{for } i \in 1,\ldots,n \tag{9}$$

Three DoFs are considered at each node, including vertical displacement v, the torsional motion θ and the shear deformation effect φ. The shape function matrix $\mathbf{N_e}$ is expressed as the Kronecker product of spectral shape function vector $\mathbf{N} = [N_1(\xi),\ldots,N_n(\xi)]^T$ and a 3 × 3 identity matrix **I**.

$$\mathbf{N_e} = \mathbf{N} \otimes \mathbf{I} \tag{10}$$

with

$$N_i(\xi) = \prod_{m=1, m\neq i}^{n} \frac{\xi - \xi_m}{\xi_i - \xi_m} \text{ for } i \in 1, \ldots, n \tag{11}$$

The stress-strain matrix and the mass density matrix $\boldsymbol{\mu}$ are expressed based on Timoshenko beam theory and elementary rod theory.

$$\mathbf{D} = \begin{bmatrix} GJ & 0 & 0 \\ 0 & K_1^{Tim} GA & 0 \\ 0 & 0 & EI \end{bmatrix} \tag{12}$$

$$\boldsymbol{\mu} = \begin{bmatrix} \rho I_o & 0 & 0 \\ 0 & \rho A & 0 \\ 0 & 0 & K_2^{Tim} \rho I \end{bmatrix} \tag{13}$$

The strain-displacement operator $\mathbf{B_e}$ is expressed as

$$\mathbf{B_e} = \begin{bmatrix} \frac{\partial}{\partial x} & 0 & 0 \\ 0 & \frac{\partial}{\partial x} & -1 \\ 0 & 0 & \frac{\partial}{\partial x} \end{bmatrix} \mathbf{N_e} = \begin{bmatrix} \frac{1}{J}\frac{\partial}{\partial \xi} & 0 & 0 \\ 0 & \frac{1}{J}\frac{\partial}{\partial \xi} & -1 \\ 0 & 0 & \frac{1}{J}\frac{\partial}{\partial \xi} \end{bmatrix} \mathbf{N_e} \tag{14}$$

By substituting $\mathbf{B_e}$, $\mathbf{D}$, $\boldsymbol{\mu}$ and $\mathbf{N_e}$ into the Eqs. (5)–(7), the element matrix of stiffness and mass, as well as the element load vector are calculated.

2.3. Cracked spectral element formulation

A cracked SFE is developed to simulate the phenomenon of torsional GW scattering and the effect of torsional-flexural coupling mode conversion when the wave interacts with the crack [46,52]. The proposed element has one node at each end with a small length, while each contains three DoFs. A schematic diagram of the spectral cracked element cross-section and time-domain SFE model is shown in Fig.2.

The cracked element stiffness matrix $\boldsymbol{K_{e,c}}$ is different from the uncracked element stiffness $\boldsymbol{K_e}$ due to the appearance of a crack and it is written as

$$\boldsymbol{K_{e,c}} = \mathbf{T}\mathbf{Q}^{-1}\mathbf{T}^{\mathrm{T}} \tag{15}$$

$\boldsymbol{T}$ and $\boldsymbol{G}$ is the transformation matrix and flexibility matrix which are given by

$$\boldsymbol{T}^T = \begin{bmatrix} 1 & 0 & 0 & -1 & 0 & 0 \\ 0 & 1 & 0 & 0 & -1 & -l \\ 0 & 0 & 1 & 0 & 0 & -1 \end{bmatrix} \tag{16}$$

$$\boldsymbol{Q} = \begin{bmatrix} q_{11} & q_{12} & q_{13} \\ q_{21} & q_{22} & q_{23} \\ q_{31} & q_{32} & q_{33} \end{bmatrix} \tag{17}$$

With

$$\begin{gathered} q_{11} = \frac{l}{GI_o} + I_{g1} + I_{g2};\ q_{22} = \frac{kl}{GA} + \frac{l^3}{3EI} + I_{g4} + s^2 I_{g3};\ q_{33} = \frac{l}{EI} + I_{g3} \\ q_{12} = q_{21} = I_{g5};\ q_{13} = q_{31} = 0;\ q_{23} = q_{32} = \frac{l^2}{2EI} + sI_{g3} \end{gathered} \tag{18}$$

where:

$$\begin{gathered} I_{g1} = \int_A \frac{8\alpha\beta^2 F_{II}^2}{\pi E\left(R^4 - r^4\right)^2} dA;\ I_{g2} = \int_A \frac{2m\alpha h^2 F_{III}^2}{\pi E\left(R^4 - r^4\right)^2} dA;\ I_{g3} = \int_A \frac{32\alpha\beta^2 F_1^2}{\pi E\left(R^4 - r^4\right)^2} dA \\ I_{g4} = \int_A \frac{2mk^2\alpha\left(R^2 + r^2\right)^2 F_{III}^2}{\pi E\left(R^4 - r^4\right)^2} dA;\ I_{g5} = \int_A \frac{2mk\alpha h\left(R^2 + r^2\right) F_{III}^2}{\pi E\left(R^4 - r^4\right)^2} dA \end{gathered} \tag{19}$$

where l is the length of the cracked element. F_I, F_{II} and F_{III} are empirical boundary calibration factors, and they can be found in [46,52]. The global stiffness matrix $\boldsymbol{K}$ is thereby calculated via the assembly procedure of combining the element cracked stiffness matrix $\boldsymbol{K_{e,c}}$ and the element uncracked stiffness matrix $\boldsymbol{K_e}$ together. The global mass matrix $\boldsymbol{M}$ and the global load vector $\boldsymbol{F}(t)$ is also constructed by assembling the corresponding element matrices. The dynamic characteristics of displacement, velocity, and acceleration can then be estimated by applying explicit central difference method to the ordinary differential equation in Eq. (4) [23]. For damage identification, the proposed SFE crack model is employed to simulate the numerical GW time-domain signal. The crack properties in Fig.2, including damage location and damage size (i.e., width and depth), are treated as uncertain parameters for calibration.

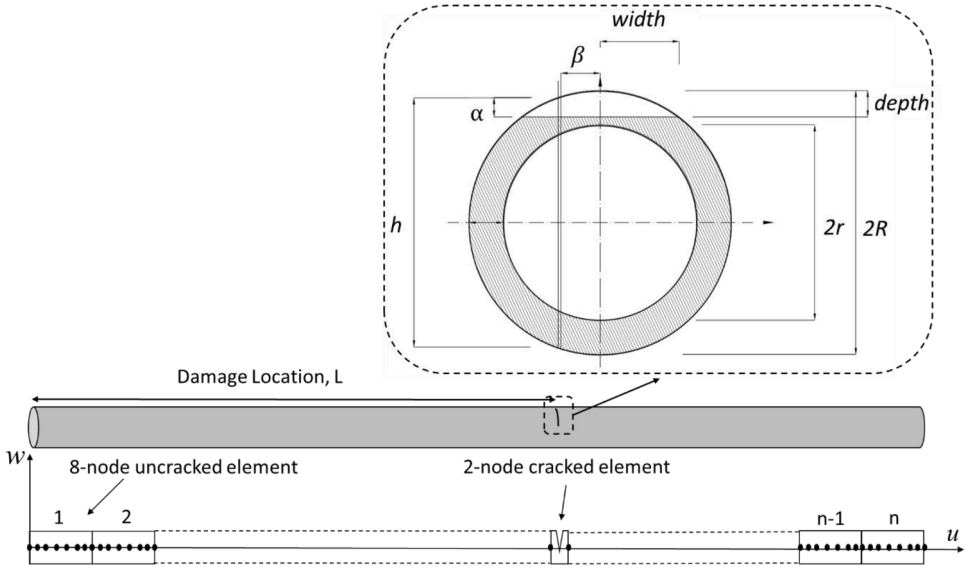

Fig. 2. A schematic diagram of the spectral cracked element cross-section and time-domain SFE model.

It should be noted that the SFE pipe model can also incorporate any type of damage in any direction depending on the practical situation. Simulation of different types of damage in the SFE model can be achieved by creating a cracked stiffness element matrix between the uncracked ones, and then adopting the corresponding analytical formulation of the transformation matrix and flexibility matrix [52]. Multiple cracks simulation can also be done by inserting the cracked stiffness element matrices into the corresponding locations. Based on the modified global stiffness matrix $\boldsymbol{K}$ and global mass matrix $\boldsymbol{M}$, the dynamic characteristics of the model are still estimated by solving the ordinary differential equation. Therefore, the overall computational efficiency of the SFE model is not affected if the model size and the time interval remain the same. In this paper, the type of crack is assumed as the axisymmetric crack along the longitudinal direction of the pipe for demonstrating the performance of the proposed Bayesian damage characterisation framework, which will be described in the following section.

3. Guided wave-based identification by approximate Bayesian computation

3.1. Approximate Bayesian computation

Consider a set of observation Y_m, let θ be the uncertain parameters of interest. The initial degree of relief about θ is expressed by the prior distribution $P(\theta)$. The prior probability density function (PDF) can be updated using the observed information in the dataset, based on Bayes' theorem:

$$P(\theta|Y_m) = \frac{P(Y_m|\theta)P(\theta)}{P(Y_m)} = \frac{P(Y_m|\theta)P(\theta)}{\int_\theta P(Y_m|\theta)P(\theta)d\theta} \tag{20}$$

where $P(\theta|Y_m)$ is the posterior PDF of the unknown parameters considering the observed data. $P(Y_m|\theta)$ is the likelihood function. $P(Y_m)$ is the evidence, which is known as a normalising constant, so-called marginal likelihood.

Approximate Bayesian Computation (ABC) is an effective alternative for solving Bayesian inference. It directly uses the similarity between measured and numerical data to approximate the posterior distribution of the model parameters, thereby replacing the evaluation of the likelihood function [34–37]. Specifically, in terms of the generic procedures of the ABC methods, a candidate parameter θ is sampled from some distribution, such as the prior for the first candidate. A numerical dataset X_s with the same geometry as Y_m is computed from the model $f(\theta, u)$, where u is some deterministic input required for model simulation.

The simulated dataset X_s is then compared with Y_m by computing a distance function $\rho(X_s, Y_m)$. For the convenience of computation, if the dimension of observation is large, the lower-dimensional vector of summary statistics $S()$ (e.g., mean, and standard) is often used, so that the distance function can also be expressed as $\rho(S(X_s), S(Y_m))$. The candidate parameter with nonzero probability is accepted if the distance function is less than desired tolerance ϵ, thereby the final output from ABC is a sample set of candidate parameters which is in the distribution of $P(\theta|\rho(X_s, Y_m) \le \epsilon)$. If ϵ is a sufficiently small value ($\epsilon \to 0$), then $X_s \to Y_m$ and hence the distribution $P(\theta|\rho(X_s, Y_m) \le \epsilon)$ can be considered as a good approximation for the desired posterior $P(\theta|Y_m)$.

A general expression of the posterior approximation using ABC can be written as follows [35]:

$$P(\theta|Y_m) = P(\theta|S(Y_m) \le \epsilon_0) \approx P(\theta|\rho(S(X_s), S(Y_m)) \le \epsilon_0) \tag{21}$$

The selection of desired tolerance reflects a trade-off between the computational cost of simulation and the approximation accuracy. The selections of distance function and summary statistics are also crucial to the posterior approximation accuracy and quality [34–37].

3.2. Subset simulation by approximate Bayesian computation

To enhance the computational efficiency for sufficiently small tolerances, ABC-SubSim is an advanced sequential algorithm that it combines the concepts of ABC with the subset simulation technique [40]. The basic idea of this algorithm is to make the simulated dataset from the numerical model closer and closer to the measured data and eventually estimate the posterior by employing a nested decreasing sequence region in the subset simulation [41,42].

Specifically, let $z = (\theta, X_s)$, so that $P(z) = P(X_s|\theta)P(\theta)$. Let also D be the nested descending sequence regions, in which the region D of possible solutions can be considered as the intersection of m nested regions:

$$D_1 \supset \ldots D_j \supset \ldots \supset D_m = D = \cap_{j=1}^{m} D_j \text{ for } j = 1, \ldots, m \tag{22}$$

with

$$D_j = \left\{(\theta, D_m) : \rho(S(X_s), S(Y_m)) \le \epsilon_j\right\} \text{ with } \epsilon_{j+1} < \epsilon_j \tag{23}$$

where ϵ_j is the intermediate tolerance at each region; m is the maximum simulation level.

The tolerance levels are adaptively decreasing in a sequence that $\epsilon_1 > \epsilon_2 > \ldots > \epsilon_m$, where the last tolerance at the simulation level of m is equal to or less than the final desired tolerance ϵ_f. The maximum simulation level is chosen in case the desired tolerance is too small [40].

By the definition of conditional probability, the probability of final region D_m can be achieved by a product of $P(D_1)$ and sequence regions of $P(D_j|D_{j-1})$.

$$P(D_m) = P(D_1)\prod_{j=2}^{m} P\left(D_j|D_{j-1}\right) \tag{24}$$

In the proposed algorithm, the samples for the probability $P(D_1)$ in the first level are estimated by a direct Monte Carlo (MC) method from the initial prior distribution of each parameter. When $j \ge 2$, the samples in the higher levels for probability $P(D_j)$ are drawn using a modified Metropolis algorithm (MMA) [41,53]. Based on the aforementioned equations, the final stage is achieved when the maximum simulation level is reached, or the intermediate tolerance ϵ_m is within the desired threshold ϵ_f, and thereby the posterior of the observation $P(\theta, Y_m|D_m)$ can be obtained.

3.3. Schematic framework for guided wave-based identification

A simplified schematic framework of the ABC-SubSim algorithm for guided wave-based damage characterisation for pipe-like structures is shown in Fig.3 for a more obvious description. Firstly, N random samples $\boldsymbol{\theta}_s$ of unknown damage characteristics are generated from the prior PDF. These samples are then input into the SFE model $f(\theta, u)$, which was presented in the previous section, to generate the corresponding simulated GW. N distance functions between the simulated and the observed GW signals $\rho(X_s, Y_m)$ are computed. In this research, to access the similarity between the simulated GW signals and the measurement, the cosine distance was chosen as the distance function [45].

$$\rho(X_s, Y_m) = 1 - \left|\frac{Y_m \cdot X_s^{'}}{\sqrt{\left(Y_m \cdot Y_m^{'}\right)\left(X_s \cdot X_s^{'}\right)}}\right| \tag{25}$$

Random samples $\boldsymbol{\theta}_s$ are sorted by rearranging the distances $\rho(X_s, Y_m)$ in an ascending order so that $\rho_{(1)} < \ldots < \rho_{(N)}$. The intermediate tolerance ϵ_j is obtained by the average distance values in the $(NP_0)th$ and the $(NP_0+1)th$ order, where P_0 is a fixed value of the conditional probability. The optimal value of P_0 is chosen as 0.2 in ABC-SubSim to improve the simulation efficiency [40]. Another alternative way to adaptively choose P_0 can be found in [54,55]. If the stopping criteria are

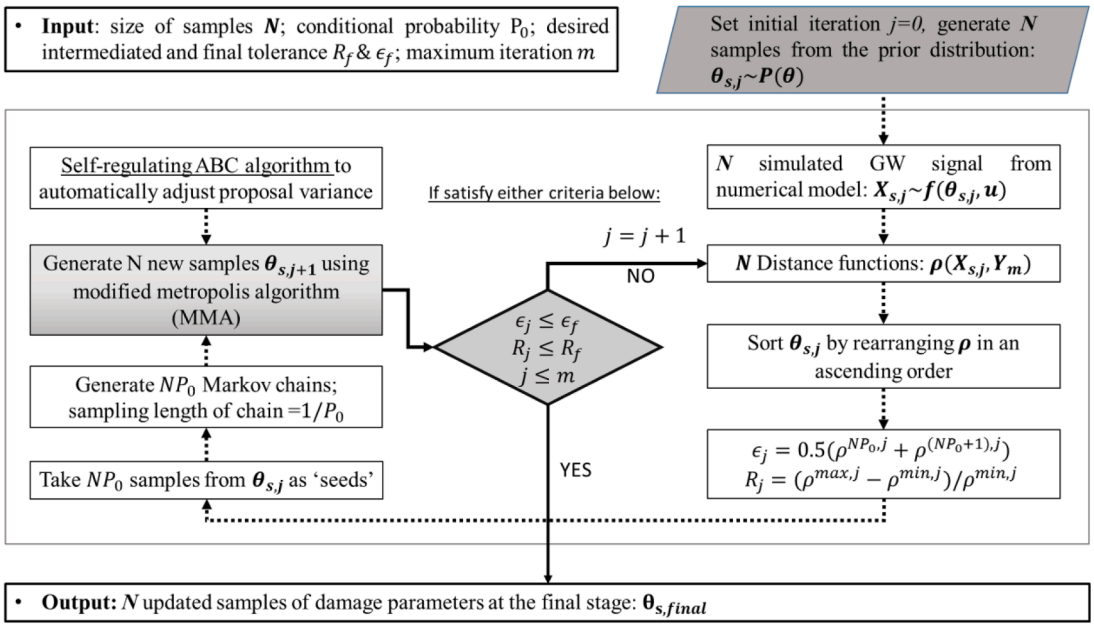

Fig. 3. A schematic flowchart for GW-based damage identification.

unsatisfied, which will describe later, NP_0 samples are selected from the available samples as 'seeds' to generate NP_0 Markov chains, while each chain has the same sampling length $1/P_0$, so that the total size of new samples set for the next step can be consistent as N. The new sample generation in each chain is based on the modified metropolis algorithm (MMA). The new sample set is used in the next iteration.

Unlike the conventional Metropolis-Hasting using multi-dimensional proposal distribution, MMA uses a univariate proposal PDF for each parameter, and each candidate is then accepted or rejected separately. The performance of MMA significantly impacts the simulation efficiency and accuracy, in which the proposal PDF in MMA plays a vital role [41, 42]. A good performance of the ABC-Subset simulation requires an acceptance rate of 30% to 50% at each level and the desired optimal value suggested in [48] is 0.44. The expected acceptance ratio is controlled by adaptively selecting the spread or variance σ in each univariate proposal PDF for each chain [53]. Nevertheless, selecting the optimal variance requires user experiences or even brute-force searches. Recently, a self-regulating proposal variance algorithm within the ABC-SubSim framework was developed by Vakilzadeh et al. [56]. It provides a more practical alternative to dynamically adjust the proposal variance in each simulation level, so that the mean acceptance rate of candidate samples can easily stay within the target value. The self-regulating ABC algorithm is hence considered in this research.

In terms of the stopping criteria, the simulation is repeated until either the maximum simulation stage m is reached, or the intermediate tolerance ϵ_j is equal to or less than the desired final threshold ϵ_f. However, setting an appropriate final threshold ϵ_f is crucial for both approximation accuracy and computational efficiency. A good posterior distribution can be approximated when the intermediate tolerance is close to 0. Nevertheless, if a too-low value of ϵ_f is used, the simulation sometimes may have reached the convergence region even though the intermediate tolerance is still larger than the desired final threshold in practice. The simulation is still running and creating un-necessary computational costs until the maximum stage m is reached. Hence, a new stopping criterion can be added to justify the convergence of samples at each stage, by accessing the difference between the lowest and the highest distance function at each sample set [57]:

$$R_j = \frac{\rho_{max,j} - \rho_{min,j}}{\rho_{min,j}} \le R_f \tag{26}$$

where R_f is the desired intermediate threshold with a relatively small value, e.g., 10^{-4}–10^{-6}.

The posterior distributions of the damage parameters are finally obtained by evaluating the sample distribution at the final stage of simulation, and thereby, the unknown damage can be identified and characterised, as well as the associated uncertainties are quantified.

4. Numerical case studies

4.1. Numerical studies setup

The performance of the proposed likelihood-free probabilistic framework is investigated in this section. An aluminium pipe with a length of 1000mm, an inner radius of 9.5mm and an outer radius of 12.5mm was used. The Poisson's ratio, mass density, and Young's modulus are 0.3, 2700kg/m^3, and 70GPa, respectively. Torsional guided wave $T(0,1)$ was generated at the left end of pipe in the rotation of longitudinal direction. The excitation was chosen as a 50kHz narrow-band 5-cycle sinusoidal tone burst modulated by a Hann window. The measured location was assumed at the same point of the excitation in all numerical cases. The time duration of the measured signal allows the incident torsional wave propagates from the excitation location to the right end, and then travels back to the initial point.

In time-domain SFE method, the time step was selected to guarantee convergence of the ordinary differential equation, which was solved by the central difference method [24]. Each uncracked SFE was simulated with a 10-mm length and 8 GLL nodes. The numerical dataset from SFE model was used for the Bayesian damage characterisation procedure.

The aluminium pipe with the described crack was also simulated using a 3D explicit FE model. The simulated time-domain signal in the same calculated location as the time-domain SFE method was treated as the synthetic experimental dataset. In this study, the commercial software, ABAQUS, was used. Brick elements C3D8R were used with a maximum element size of 0.8 mm. The thickness for the finite elements is 0.6 mm, so the pipe wall simulation has at least five elements in the thickness direction. The crack is 1 mm in width in the longitudinal direction. Different damage severities were modelled by removing the elements at the corresponding location. Four different scenarios, i.e., i) standard case, ii) different measurement noise levels, iii) different cracked locations, and iv) crack severity analysis, as shown in Table 1,

Table 1
Summary of all numerical case studies.

Numerical study Scenario	Case	Location, L (mm)	Crack depth, d (mm)	Crack width, w (mm)	Young's modulus, E (GPa)	Noise level (%)
Standard case	A1	350.00	2.01	6.80	–	2.00
	A2	350.00	2.01	6.80	70.00	2.00
Measurement noise level effect	B1	350.00	2.01	6.80	70.00	1.00
	B2	350.00	2.01	6.80	70.00	3.00
	B3	350.00	2.01	6.80	70.00	5.00
Different locations	C1	500.00	2.01	6.80	70.00	2.00
	C2	700.00	2.01	6.80	70.00	2.00
Different crack sizes	D1	350.00	1.73	6.35	70.00	2.00
	D2	350.00	2.20	7.00	70.00	2.00
	D3	350.00	2.81	7.89	70.00	2.00

were used to investigate the performance of likelihood-free damage characterisation method comprehensively.

In the probabilistic framework, it was assumed that the crack does not penetrate the pipe wall due to early-stage damage detection, and there is no available information regarding the pipe. Thereby, the prior PDF for each parameter was chosen as independently uniformly distributed over the ranges [0 mm 1000 mm], [0 mm 3 mm], and [0 mm 8.124 mm] for damage location, width, and depth, respectively.

In addition, the modelling error should be appropriately considered as the potential uncertainty. Considering that pipe geometry and density can be measured accurately, while Young's modulus may vary depending on pressure and temperature. Thereby, Young's modulus of aluminium pipe is assumed as an uncertain parameter for calibration, with a uniform distribution ranging from 67 *GPa* to 73 *GPa*. This study also considered measurement error by simulating different levels of signal-to-noise ratio to the synthetic experimental dataset from 3D finite element (FE) model. The number of samples N of the ABC-SubSim algorithm was set at 500. The conditional probability P_0 was 0.2. The desired final threshold ϵ_f and the desired intermediate threshold R_f were chosen as 10^{-3} and 10^{-5}, respectively. The optimal acceptance rate was chosen as 0.44 for the self-regulating ABC algorithm in each stage [56].

4.2. Standard case

Case A is used to investigate the performance of subset simulation with a self-regulating ABC algorithm. In the following numerical case studies, Case A is also the nominal case for comparison. If a crack exists, the mode conversion effect of the torsional-flexural (T-F) wave occurs when the incident torsional $T(0,1)$ wave interacts with the crack. Both numerical and experimental validation has been conducted for the proposed time-domain SFE method [46]. For illustration, details of time-domain reflected signals measurements for Case A simulated by the proposed SFE model and 3D FE model are shown in Fig. 4. Figs. 4(a) and 4(b) show the signal without noise and with artificial 2% signal-to-noise level.

Both calculated datasets are normalised by dividing by the maximum amplitude of the whole simulated GW signal. A good agreement of calculated reflected signals between FE model and SFE model is observed. The reflected wave signal contain the information of incident torsional T(0,1) wave, T-T(0,1) wave due to crack, as well as the mode converted T-F(0,1) wave due to crack. Time-of-arrival of waves is different because of different propagation velocities and distances. The incident T-T wave propagates back from the right pipe end is excluded from the measured signal to save computational costs.

The mode-conversion effect of crack provides extra information about crack [24]. Hence it was also considered in the damage identification. The damage location can usually be determined based on the scattered wave of time-of-flight from the defect to the measured point. The severity of the damage can be estimated by evaluating scattered wave amplitude. As shown in Table 2, both the mean and the corresponding coefficient of variation (COV) value of Case A1 show low percentage values, which shows that the crack parameters are accurately identified with only a low level of uncertainty.

Young's modulus is another unknown parameter for updating by considering the material modelling error. Changes in material property can be reflected in the variation of GW propagation velocity. As the updated results of Case A2 in Table 2, crack parameters can still be precisely identified under an acceptable noise condition, while E can be determined with only 0.03% errors.

The scatter plots of 500 samples of the defect location and depth at different stages in Case A2 are shown in Fig. 5 for illustration. Stage 1 was the initial stage of the proposed framework where the samples were randomly drawn from the prior distribution of the parameters. When the

Table 2
Cases A1-A2: Identified results and corresponding COVs.

Numerical Case		Location, L (mm)	Crack depth, d (mm)	Crack width, w (mm)	Young's modulus, E (GPa)
A1	Actual	350.00	2.01	6.80	–
	Sample mean [error %]	350.02 [0.01]	2.01 [0.03]	6.80 [0.02]	–
	Sample COV (%)	0.01	0.52	0.25	–
A2	Actual	350.00	2.01	6.80	70.00
	Sample mean [error %]	350.03 [0.01]	2.01 [0.03]	6.80 [0.02]	69.98 [0.03]
	Sample COV (%)	0.02	0.50	0.11	1.14

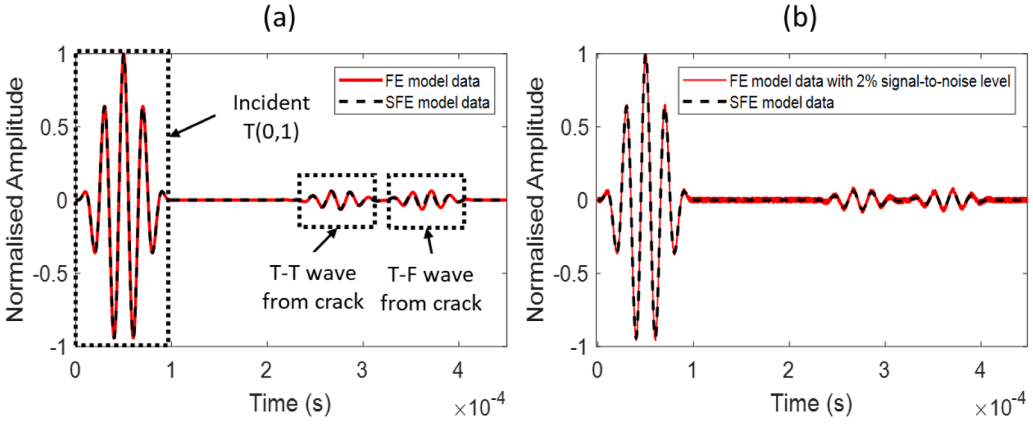

Fig. 4. Calculated time-domain signals simulated by FE model and SFE model (a) noise-free and (b) with 2.0% artificial signal-to-noise level.

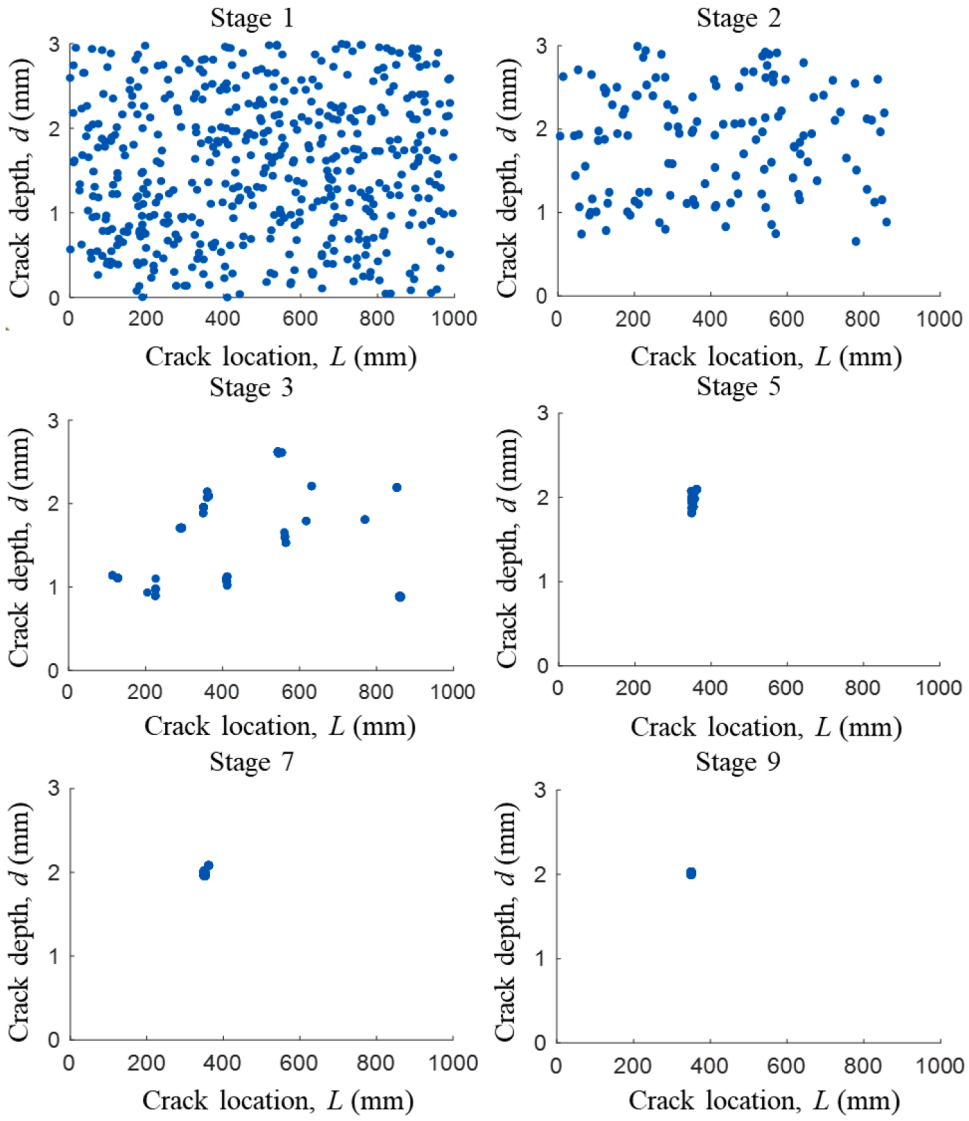

Fig. 5. Scatter plots of the samples for the location and depth of crack in Case A2.

stage number increased, the scattering area of ABC-SubSim samples became smaller, indicating that the sample movements gradually converged together to the global optimal region. The intermediate tolerance level ϵ_j, which was determined based on the sample distance function set (see Fig.3), was also adaptively decreasing with the iteration. The simulation was eventually stopped at Stage 9 as the desired final threshold was reached that $\epsilon_9 \leq \epsilon_f$. The final posterior distributions of the damage parameters were obtained. All 500 samples at Stage 9 were accurately scattered around the actual value of the defect location and depth, the results indicate the accuracy and robustness of the proposed Bayesian framework in crack identification.

Fig.6 shows the histograms for each crack parameter at the final stage in Case A2. The estimated posterior distribution of each parameter is well-establish around the actual value. The results again indicate that the crack characteristics and Young's modulus are accurately identified, while the corresponding uncertainties are also quantified with an expected level under the artificial measurement noise.

4.3. Measurement noise levels

This section investigates the performance of the likelihood-free probabilistic framework under different measurement noise conditions. The noise level domain from 1% to 5% is determined under normal experimental laboratory conditions. As shown in Table 3, the updated values indicate that the model unknowns are still correctly identified. Both error percentages of the sample mean and COV showed an increasing tendency with the noise levels as expected. For example, the COV value of E increased from 0.68% to 4.45% with the increasing noise level. The crack depth and width error percentages also increased from 0.03 to 0.31 and from 0.02 to 0.18, respectively. The results also demonstrate that the measurement noise would cause different impacts on each individual parameter, which leads to different trends in the magnitude of the uncertainty quantification.

4.4. Different locations of cracks

The influence of crack location is also investigated. The damage severity is the same as the standard case, except for the damage location. In terms of the quantified uncertainty, both error percentages of sample mean and COV value is larger than in Case A, especially in Case C2. For example, the mean error of location L increased from 0.01% to 0.52% when the measurement distance was double the initial ones. The COV value of E also raised from 1.11 to 4.53%. The results illustrate that due to the longer propagation distance of the scattered GW wave from the defect to the measurement point, more noise errors would be accumulated in the time-domain signal as expected, and hence, lead to more

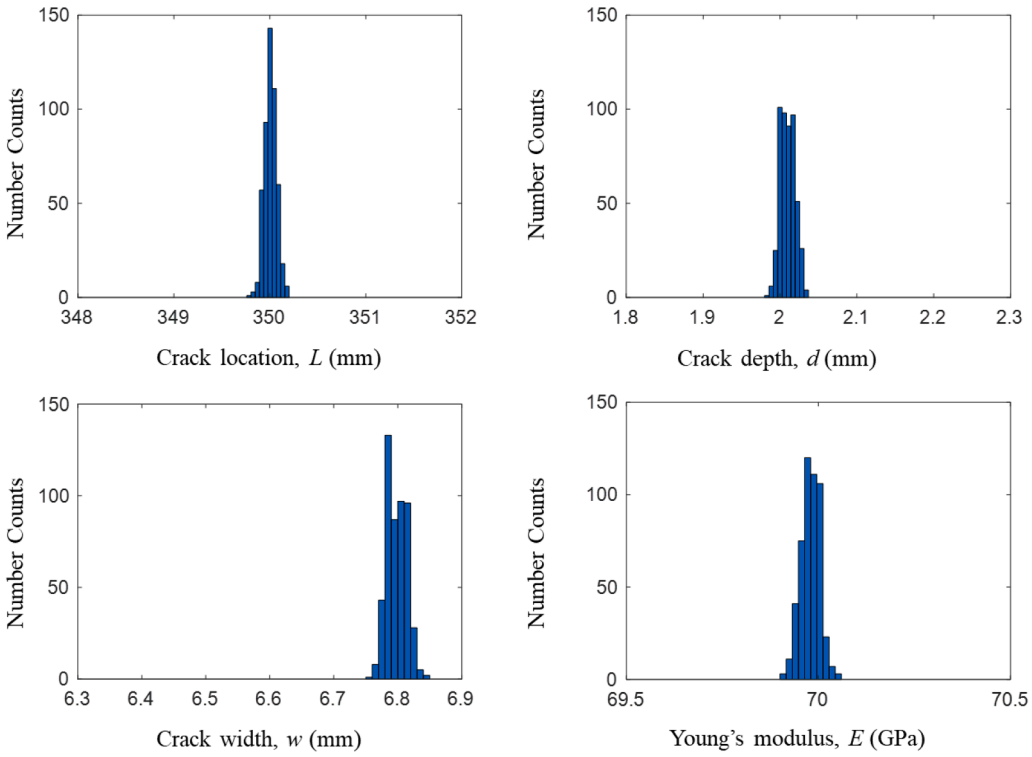

Fig. 6. Histograms of the final samples for each parameter in Case A2.

Table 3
Cases B1-B3: Identified results and corresponding COVs.

Numerical Case		Location, L (mm)	Crack depth, d (mm)	Crack width, w (mm)	Young's modulus, E (GPa)
Actual		350.00	2.01	6.80	70.00
B1	Sample mean [error %]	349.93 [0.02]	2.01 [0.03]	6.80 [0.02]	69.99 [0.01]
	Sample COV (%)	0.01	0.34	0.08	0.68
B2	Sample mean [error %]	349.58 [0.12]	2.01 [0.17]	6.80 [0.05]	70.23 [0.33]
	Sample COV (%)	0.06	0.47	0.11	3.47
B3	Sample mean [error %]	349.68 [0.09]	2.00 [0.31]	6.79 [0.18]	70.24 [0.33]
	Sample COV (%)	0.08	0.67	0.15	4.45

Table 4
Cases C1-C2: Identified results and corresponding COVs.

Numerical Case		Location, L (mm)	Crack depth, d (mm)	Crack width, w (mm)	Young's modulus, E (GPa)
C1	Actual	500.00	2.01	6.80	70.00
	Sample mean [error %]	500.00 [0.01]	2.01 [0.16]	6.80 [0.04]	70.00 [0.01]
	Sample COV (%)	0.01	1.35	0.31	1.11
C2	Actual	700.00	2.01	6.80	70.00
	Sample mean [error %]	703.67 [0.52]	2.02 [0.39]	6.81 [0.15]	70.05 [0.07]
	Sample COV (%)	0.10	0.96	0.22	4.53

uncertainty involve in the damage identification simulation. Nevertheless, as summarised in Table 4, the model parameters are still correctly identified which reflects the robustness of the proposed damage characterisation framework.

4.5. Different crack severity

The severity of a damage is usually estimated based on the amplitude of the scattered waves from the defect. The reflection coefficient of guided wave is proportional to the radial cross-section area of the axisymmetric crack [46]. It is also expected that the difficulty of crack severity detection would increase with the measurement of noise levels. In this section, an axisymmetric crack is simulated with a constant 1 mm width in longitudinal direction. The effect of the crack severity in radial direction is examined from Cases D1 to D4 under 2% synthetised noise level.

Table 5 summarises all updated results with the corresponding mean errors and sample COV values. The model parameters for Cases D1 to D3 are correctly identified when the crack size is over half of the pipe wall. The results illustrate that the accuracy of crack identification is improved under the same measurement noise level when the reflected energy of the scattering wave from the defect is higher due to the larger size of the crack.

In this numerical study, three different scenarios were carried out to investigate the GW based damage characterisation framework in pipes using torsional waves. In terms of accuracy, the uncertain parameters of the SFE pipe model were correctly identified and characterised in each case study. In particular, the accuracy is improved with a larger crack size as discussed in Section 4.5. These results reflect the robustness and feasibility of the proposed likelihood-free approach in identifying the cracks. In addition, the associated uncertainty of each parameter was quantified by calculating the mean and COV values, which provided additional information regarding the reliability of the results. It was also found that under different scenarios, the quantified uncertainty is

Table 5
Cases D1-D3: Identified results and corresponding COVs.

Numerical Case		Location, L (mm)	Crack depth, d (mm)	Crack width, w (mm)	Young's modulus, E (GPa)
D1	Actual	350.00	1.73	6.35	70.00
	Sample mean [error %]	349.98 [0.01]	1.73 [0.29]	6.34 [0.16]	69.99 [0.01]
	Sample COV (%)	0.02	0.47	0.09	2.63
D2	Actual	350.00	2.20	7.08	70.00
	Sample mean [error %]	349.96 [0.01]	2.21 [0.21]	7.09 [0.13]	69.98 [0.02]
	Sample COV (%)	0.04	0.37	0.09	2.54
D3	Actual	350.00	2.81	7.89	70.00
	Sample mean [error %]	349.96 [0.01]	2.81 [0.04]	7.88 [0.16]	70.01 [0.01]
	Sample COV (%)	0.04	0.05	0.01	2.87

increased with the noise level, different parameters have different sensitivities to the noise effect, which results in different levels of quantitative uncertainty.

5. Experimental case studies

5.1. Experimental setup

One-metre-long 6060 aluminium pipes with identical geometric and material properties as the numerical study were used to further investigate the performance of the likelihood-free probabilistic framework in practice. Material properties are summarised in Table 6.

Four evenly spaced piezoceramic shear plates were bonded to the outer surface of the pipe at the left end using conductive adhesive epoxy. The dimensions of each shear plate are $6\times 5\times 0.5\ mm^3$. The shear orientation of the PZTs is along the circumferential direction to generate the incident torsional wave.

The same excitation signal as the numerical case, a 50 kHz narrowband 5-cycle sinusoidal tone burst modulated by a Hann window, was synthesised by a signal generator NI PXIE-5122. The signal was fed into the PZTs after being amplified by the high-voltage power amplifier Ciprian. The measurement location was 200 mm away from the location of PZTs. To improve the observation quality, the 3D laser Doppler vibrometer is employed to measure the GW displacement signal. The reflected spray was also coated on the outer surface of the pipe around the measurement point to enhance laser reflection. In addition, 1000 times signal-average and low-pass filters were set further to minimise the noise impact from the experimental environment. A 1mm-width notch was created on a pipe using a tiny fine pull-cut saw blade. A specific flowchart of the experiment is summarised in Fig.7 and details of the pipe is shown in Fig.8. The detailed information of crack parameters is summarised in Table 7.

5.2. Experimental results and discussions

Three cases, Cases E1 to E3, were carried out to experimentally investigate the proposed probabilistic framework. The same set-up of framework used in the numerical case study. 500 samples N was used at each iteration in the ABC-SubSim algorithm. The conditional probability P_0 and the optimal acceptance rate was 0.2 and 0.44, respectively. The desired final threshold ϵ_f and the desired intermediate threshold R_f were selected as 10^{-3} and 10^{-5}, respectively. The same setting of prior distribution as the numerical case setting was used for each unknown parameter.

The identified results with the corresponding quantified uncertainties are summarised in Table 8. The results show that each unknown parameter is accurately detected around the actual value with low error percentages in both Sample means and COVs. This proves that the unknown damage location, severity, and material property E can be identified in practice situation using the proposed probabilistic framework.

For illustration, the scatterplot of 500 samples of crack location and depth in experimental case E2 is shown in Fig. 9. Different stages are chosen to show how the samples move from the prior distribution of the damage parameters to the posterior distribution. Firstly, at initial stage 1, 500 samples were randomly drawn from the prior distribution of the parameters using the direct Monte Carlo method. After that, the ABC-SubSim samples moved efficiently from the large scattering area to several local optimum regions as shown at Stage 5. The samples then converged to the region of global optimum at Stage 7. The area of global optimum region shown at Stage 7 was gradually minimised to the region shown at stage 10, indicating that the differences between simulated GW signals and measurement were reducing. In this experimental case, although the intermediate tolerance ϵ_{10} is still larger than the desired final threshold ϵ_f, the simulation was stopped at the Stage 10 based on the desired intermediate threshold R_f in the proposed framework (i.e., $R_{10}\leq R_f$), so that the computational efficiency was maximised. The updated values of damage parameters were obtained by evaluating the posterior distributions at the final Stage 10 and the results were correctly identified with acceptable uncertainty.

The comparison between SFE model using identified results and experimental data in Case E2 is also presented in Fig.10. to illustrate how well the damage identification is in a practical situation. A good agreement has been presented between the measured guided wave signal and the numerical signal. The T-T wave reflected from the left end of the pipe was mixed with the T-F wave from a crack in the experiment, while the numerical signal using updated results also showed the same phenomenon. It should be noted that a small magnitude of flexural wave package $F(1,1)$ was also generated following the incident $T(0,1)$ in experimental data due to the imperfect PZTs installation. Nonetheless, it can be treated as noise uncertainty in the Bayesian probability framework because of its low incident amplitude and negligible reflection from the crack. It is also observed that the noise level of measurement was well-controlled outside of the small wave package, allowing accurate damage characteristics identification for each parameter.

The histogram of 500 samples at the final stage for each parameter in case E2 are also presented in Fig.11. Although the actual value of each parameter is not within the posterior distribution, the identified results are still very close to the actual values with minor errors. Hence this can prove that the crack characteristics and Young's modulus are correctly identified using the proposed likelihood-free framework. The corresponding uncertainties are also quantified with an expected low level, which is consistent with the calculated sample mean and samples COVs in Table 8 and also the observation from Fig.9. and Fig.10.

Table 6
Properties of the 1-metre length aluminium pipe.

Properties	Outer radius (mm)	Inner radius (mm)	Young's modulus (GPa)	Poisson's Ratio	Shear Modulus (GPa)	Density (kg/m^3)
Value	12.50	9.50	70.00	0.30	26.92	2700.00

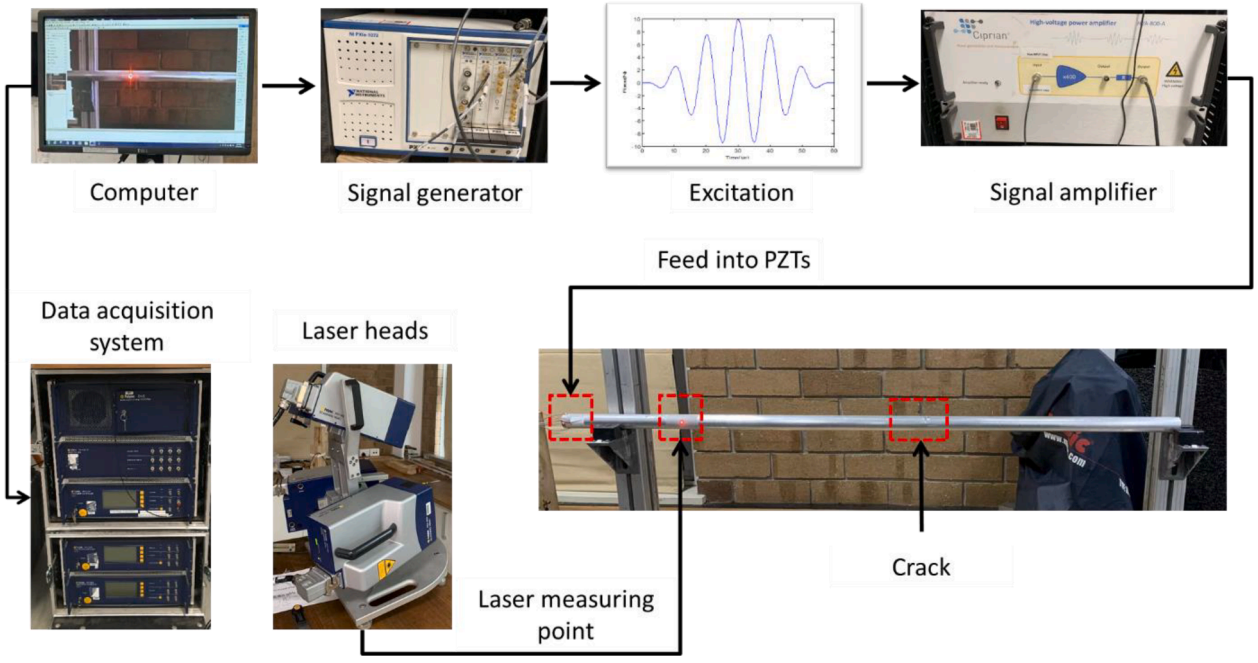

Fig. 7. A specific flowchart of the experiment.

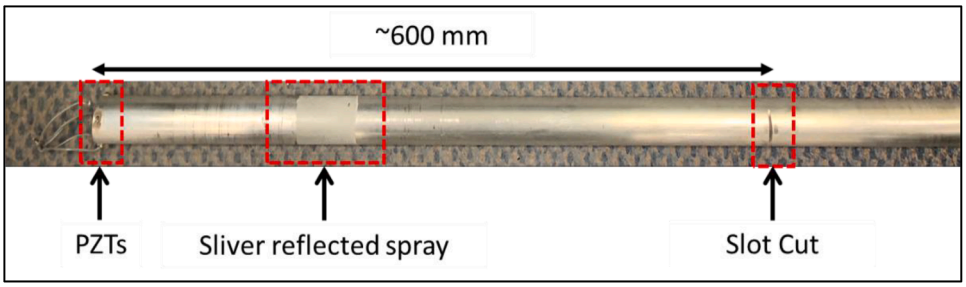

Fig. 8. PZTs for generating Torsional wave and laser measurement region, and location of the slot cut in E2&E3.

Table 7
Summary of all of the cases in the experimental case studies.

Experimental case	Location, L (mm)	Crack depth, d (mm)	Crack width, w (mm)	Young's modulus, E (GPa)
E1	500±10	1.9	6.60	70.00
E2	600±10	1.9	6.60	70.00
E3	600±10	2.9	8.01	70.00

Table 8
Identified results and corresponding COVs for Cases E1-E3.

Numerical Case		Location, L (mm)	Crack depth, d (mm)	Crack width, w (mm)	Young's modulus, E (GPa)
E1	Actual	500±10	1.9	6.60	70.00
	Sample mean [error %]	489.82 [2.04]	1.97 [3.68]	6.73 [1.97]	69.93 [0.10]
	Sample COV (%)	0.04	0.98	0.22	1.75
E2	Actual	600±10	1.9	6.60	70.00
	Sample mean [error %]	606.14 [1.02]	1.86 [2.34]	6.56 [0.68]	69.80 [0.28]
	Sample COV (%)	0.03	0.37	0.07	1.71
E3	Actual	600±10	2.9	8.01	70.00
	Sample mean [error %]	608.12 [1.35]	2.91 [0.30]	8.02 [0.12]	70.23 [0.33]
	Sample COV (%)	0.04	0.32	0.09	1.64

6. Conclusions

In this paper, a likelihood-free probabilistic framework for guided wave-based damage characterisation in pipes has been presented. The proposed damage identification framework is based on subset simulation by approximate Bayesian computation, a likelihood-free Bayesian approach. This algorithm provides an alternative way to estimate the posterior distributions of damage parameters by directly assessing the discrepancy between the simulated GW signals from the numerical model and the measured data. In this case, the evaluation of likelihood functions can be smartly bypassed during Bayesian inference. The time-domain SFE method was used for pipes to improve the computational efficiency of numerical simulation. The SFE model is developed based on Timoshenko beam theory and elementary rod theory. In addition, a cracked spectral finite element is embedded into the SFE method, which considers the mode-conversion effect of torsional-flexural mode due to the scattering wave interacting with the crack.

Numerical studies have been used to investigate the performance of the proposed framework in damage identification. The influences of material and measurement uncertainties have been examined in detail. The numerical results have demonstrated that the proposed likelihood-

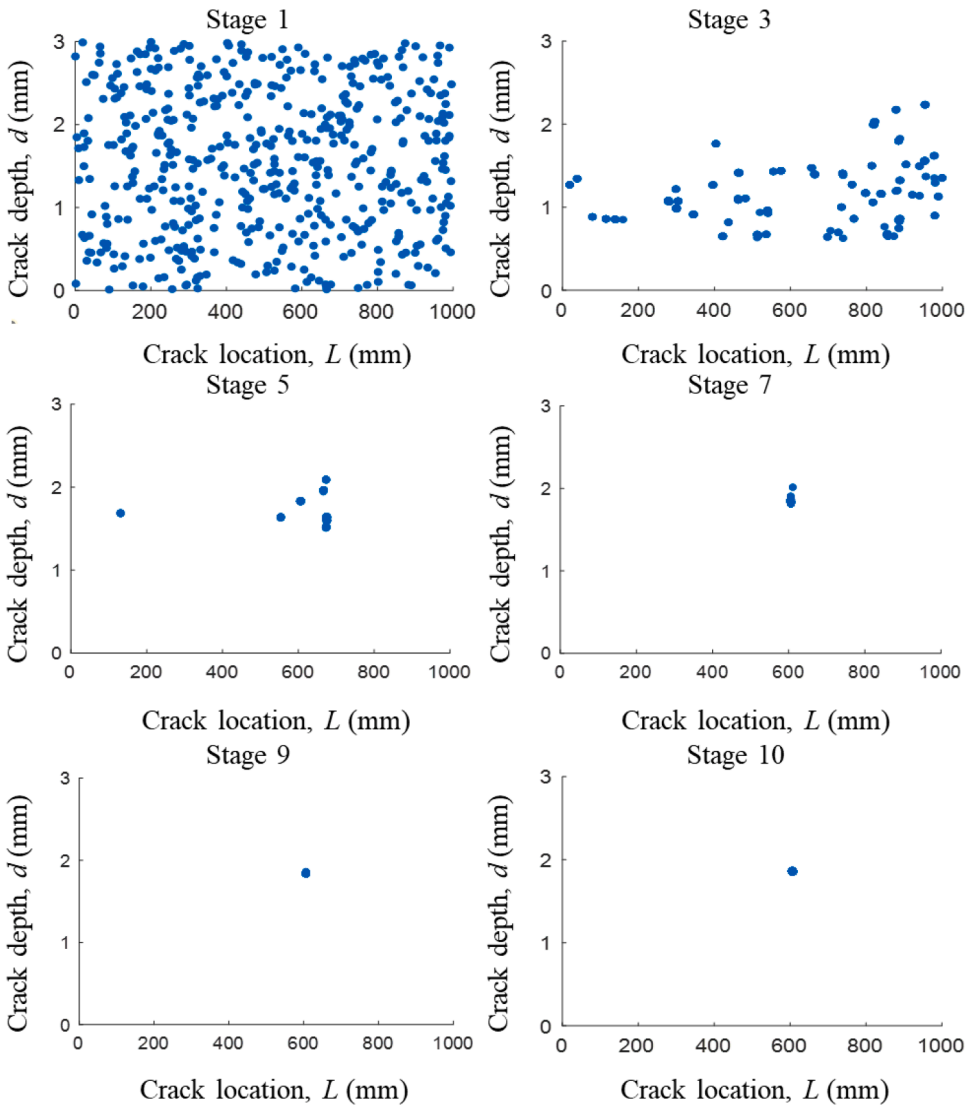

Fig. 9. Scatter plots of the samples for the location and depth of crack in Case E2.

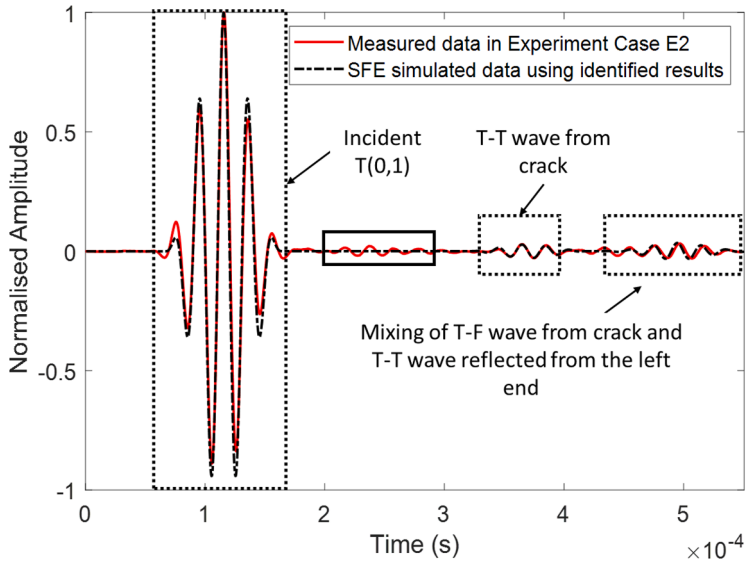

Fig. 10. Comparison of the measured and simulated time-domain GW signal for Case E2.

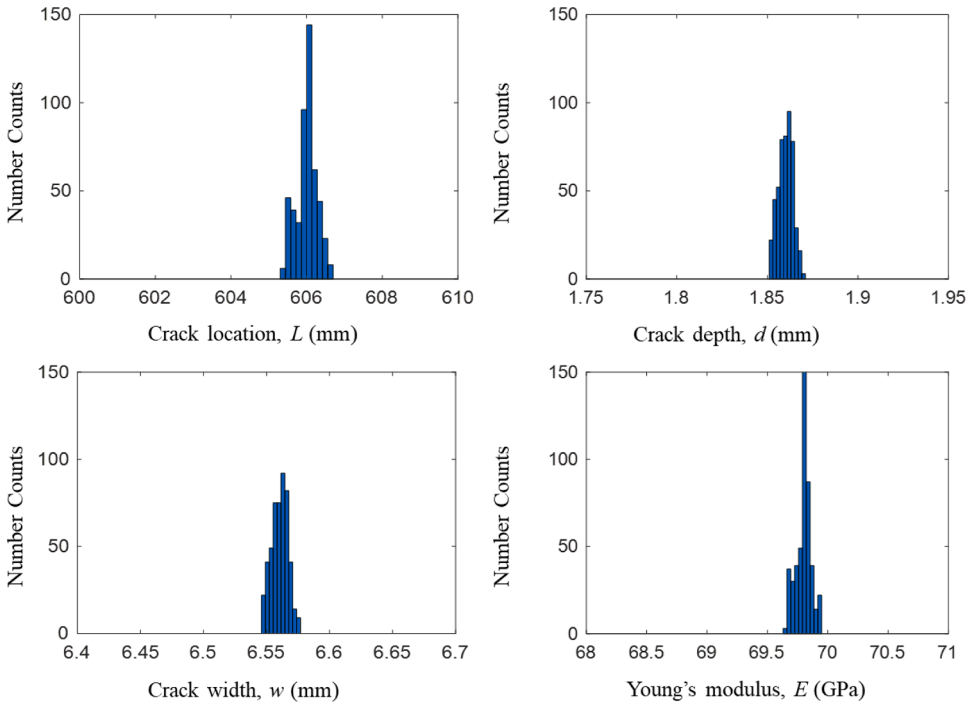

Fig. 11. Histograms of the final samples for each parameter in Case E2.

free Bayesian framework is able to identify damage characteristics and Young's modulus of the pipe under an acceptable noise condition. Finally, experimental studies have also conducted, and the experimental results have further verified the capability and practicability of the proposed damage identification algorithm in a laboratory application.

The present framework has a great potential for detecting and identifying damages in thin-walled and hollow-cylindrical structures, such as transportation pipes of fluid or gas, and columns. However, the current study is only based on an isotropic pipe model. For real-life structures, more complicated simulation models are expected. The proposed ABC technique can be used with any simulation models, but further research is required to investigate the performance of the proposed likelihood-free framework in real applications to extend its practicability. Further research can also extend the current study to damage identification and classification by employing other types of damage model to the SFE pipe model. The findings of this study have provided insights into the development of GW based damage characterisation techniques using a Bayesian likelihood-free approach. The presented framework can be used for other types of materials or structures, such as composite structures, material interfaces, or connections.

CRediT authorship contribution statement

Zijie Zeng: Writing – original draft, Validation, Methodology, Investigation, Formal analysis, Conceptualization. **Min Gao:** Validation, Formal analysis. **Ching Tai Ng:** Writing – review & editing, Supervision, Conceptualization. **Abdul Hamid Sheikh:** Writing – review & editing, Supervision.

Declaration of Competing Interest

The authors declare that they have no known competing financial interests or personal relationships that could have appeared to influence the work reported in this paper.

Data availability

Data will be made available on request.

Acknowledgement

This work was funded by the Australia Research Council (ARC) under grant numbers DP210103307 and LP210100415. The supports are greatly appreciated.

References

[1] H. Sohn, et al., A Review of Structural Health Monitoring literature: 1996–2001, 1, Los Alamos National Laboratory, USA, 2003.
[2] R. Hou, Y. Xia, Review on the new development of vibration-based damage identification for civil engineering structures: 2010–2019, J. Sound Vib. 491 (2021), 115741.
[3] Z. Su, L. Ye, Y. Lu, Guided Lamb waves for identification of damage in composite structures: a review, J. Sound Vib. 295 (3–5) (2006) 753–780.
[4] D. Montalvao, N.M.M. Maia, A.M.R. Ribeiro, A review of vibration-based structural health monitoring with special emphasis on composite materials, Shock Vib. Dig. 38 (4) (2006) 295–324.
[5] Y.K. An, H. Sohn, Integrated impedance and guided wave based damage detection, Mech. Syst. Signal. Process 28 (2012) 50–62.
[6] R. Guan, et al., Guided waves for damage identification in pipeline structures: a review, Struct. Control Health Monitor. 24 (11) (2017) e2007.
[7] C.T. Ng, Bayesian model updating approach for experimental identification of damage in beams using guided waves, Struct. Health Monitor. 13 (4) (2014) 359–373.
[8] H. Cho, C.J. Lissenden, Structural health monitoring of fatigue crack growth in plate structures with ultrasonic guided waves, Struct. Health Monitor. 11 (4) (2012) 393–404.
[9] X. Hu, C.T. Ng, A. Kotousov, Early damage detection of metallic plates with one side exposed to water using the second harmonic generation of ultrasonic guided waves, Thin Walled Struct. 176 (2022), 109284.
[10] A. Løvstad, P. Cawley, The reflection of the fundamental torsional mode from pit clusters in pipes, NDT & E International 46 (2012) 83–93.
[11] K. Papadopoulou, et al., An evaluation of acoustic reflectometry for leakage and blockage detection, in: Proceedings of the Institution of Mechanical Engineers, Part C: Journal of Mechanical Engineering Science 222, 2008, pp. 959–966.
[12] B. Chegeni, S. Jayasuriya, S. Das, Effect of corrosion on thin-walled pipes under combined internal pressure and bending, Thin Walled Struct. 143 (2019), 106218.
[13] Z. Zhang, L. Guo, Y.F. Cheng, Interaction between internal and external defects on pipelines and its effect on failure pressure, Thin Walled Struct. 159 (2021), 107230.
[14] P. Zhao, et al., Burst pressure of thin-walled pipes with dent and gouge defects, Thin Walled Struct. 159 (2021), 107213.
[15] M.J. Lowe, D.N. Alleyne, P. Cawley, Defect detection in pipes using guided waves, Ultrasonics 36 (1–5) (1998) 147–154.
[16] A. Demma, et al., The reflection of the fundamental torsional mode from cracks and notches in pipes, J. Acoust. Soc. Am. 114 (2) (2003) 611–625.

[17] P. Cawley, R.D. Adams, The location of defects in structures from measurements of natural frequencies, J. Strain Anal. Eng. Design 14 (2) (1979) 49–57.
[18] A. Løvstad, P. Cawley, The reflection of the fundamental torsional guided wave from multiple circular holes in pipes, NDT & E Int. 44 (7) (2011) 553–562.
[19] H. Kwun, et al., Torsional guided-wave attenuation in coal-tar-enamel-coated, buried piping, Ndt & E Int. 37 (8) (2004) 663–665.
[20] Q. Huan, M. Chen, F. Li, Long-distance structural health monitoring of buried pipes using pitch-catch T (0, 1) wave piezoelectric ring array transducers, Ultrasonics 106 (2020), 106162.
[21] A. Pau, F. Vestroni, Wave propagation in one-dimensional waveguides for damage characterization, J. Intell. Mater. Syst. Struct. 22 (16) (2011) 1869–1877.
[22] M. Krawczuk, Application of spectral beam finite element with a crack and iterative search technique for damage detection, Finite Elem. Anal. Des. 38 (6) (2002) 537–548.
[23] S. He, C.T. Ng, A probabilistic approach for quantitative identification of multiple delaminations in laminated composite beams using guided waves, Eng. Struct. 127 (2016) 602–614.
[24] S. He, C.T. Ng, Guided wave-based identification of multiple cracks in beams using a Bayesian approach, Mech. Syst. Signal. Process 84 (2017) 324–345.
[25] J.L. Beck, L.S. Katafygiotis, Updating models and their uncertainties. I: bayesian statistical framework, J. Eng. Mech.Proc. ASCE 124 (4) (1998) 455–462.
[26] L.S. Katafygiotis, J.L. Beck, Updating models and their uncertainties. II: model identifiability, J. Eng. Mech. 124 (4) (1998) 463–467.
[27] K.V. Yuen, S.C. Kuok, Bayesian methods for updating dynamic models, Appl. Mech. Rev. 64 (1) (2011).
[28] Y. Huang, et al., State-of-the-art review on Bayesian inference in structural system identification and damage assessment, Adv. Struct. Eng. 22 (6) (2019) 1329–1351.
[29] H. Lam, et al., Application of the spatial wavelet transform and Bayesian approach to the crack detection of a partially obstructed beam, Thin Walled Struct. 43 (1) (2005) 1–21.
[30] G. Yan, A Bayesian approach for damage localization in plate-like structures using Lamb waves, Smart Mater. Struct. 22 (3) (2013), 035012.
[31] S. Cantero-Chinchilla, et al., Bayesian damage localization and identification based on a transient wave propagation model for composite beam structures, Compos. Struct. 267 (2021), 113849.
[32] W.J. Yan, et al., A fast bayesian inference scheme for identification of local structural properties of layered composites based on wave and finite element-assisted metamodeling strategy and ultrasound measurements, Mech. Syst. Signal. Process 143 (2020), 106802.
[33] H. Wang, et al., A Bayesian model framework for calibrating ultrasonic in-line inspection data and estimating actual external corrosion depth in buried pipeline utilizing a clustering technique, Struct. Saf. 54 (2015) 19–31.
[34] J.M. Marin, et al., Approximate Bayesian computational methods, Stat. Comput. 22 (6) (2012) 1167–1180.
[35] B.M. Turner, T. Van Zandt, A tutorial on approximate Bayesian computation, J. Math. Psychol. 56 (2) (2012) 69–85.
[36] M.A. Beaumont, Approximate bayesian computation, Annu. Rev. Stat. Appl. 6 (2019) 379–403.
[37] J. Lintusaari, et al., Fundamentals and recent developments in approximate Bayesian computation, Syst. Biol. 66 (1) (2017) e66–e82.
[38] A.B. Abdessalem, et al., Model selection and parameter estimation in structural dynamics using approximate Bayesian computation, Mech. Syst. Signal. Process 99 (2018) 306–325.
[39] S.E. Fang, et al., Probabilistic damage identification incorporating approximate Bayesian computation with stochastic response surface, Mech. Syst. Signal. Process 128 (2019) 229–243.
[40] M. Chiachio, et al., Approximate Bayesian computation by subset simulation, SIAM J. Sci. Comput. 36 (3) (2014) A1339–A1358.
[41] S.K. Au, J.L. Beck, Estimation of small failure probabilities in high dimensions by subset simulation, Probab. Eng. Mech. 16 (4) (2001) 263–277.
[42] S.K. Au, J. Ching, J. Beck, Application of subset simulation methods to reliability benchmark problems, Struct. Saf. 29 (3) (2007) 183–193.
[43] P. Marjoram, et al., Markov chain Monte Carlo without likelihoods, Proc. Natl. Acad. Sci. 100 (26) (2003) 15324–15328.
[44] S.A. Sisson, Y. Fan, M.M. Tanaka, Sequential monte carlo without likelihoods, Proc. Natl. Acad. Sci. 104 (6) (2007) 1760–1765.
[45] M.A. Fakih, et al., A Bayesian approach for damage assessment in welded structures using Lamb-wave surrogate models and minimal sensing, NDT & E Int. 128 (2022), 102626.
[46] C. Yeung, C.T. Ng, Time-domain spectral finite element method for analysis of torsional guided waves scattering and mode conversion by cracks in pipes, Mech. Syst. Signal. Process 128 (2019) 305–317.
[47] M. Petyt, Introduction to Finite Element Vibration Analysis, Cambridge university press, 2010.
[48] J.F. Doyle, Wave Propagation in structures, in Wave propagation in Structures, Springer, 1989, pp. 88–125.
[49] M. Rucka, Experimental and numerical studies of guided wave damage detection in bars with structural discontinuities, Arch. Appl. Mech. 80 (2010) 1371–1390.
[50] S. He, C.T. Ng, Modelling and analysis of nonlinear guided waves interaction at a breathing crack using time-domain spectral finite element method, Smart Mater. Struct. 26 (8) (2017), 085002.
[51] P. Kudela, M. Krawczuk, W. Ostachowicz, Wave propagation modelling in 1D structures using spectral finite elements, J. Sound Vib. 300 (1–2) (2007) 88–100.
[52] A. Darpe, K. Gupta, A. Chawla, Coupled bending, longitudinal and torsional vibrations of a cracked rotor, J. Sound Vib. 269 (1–2) (2004) 33–60.
[53] K.M. Zuev, et al., Bayesian post-processor and other enhancements of Subset Simulation for estimating failure probabilities in high dimensions, Comput. Struct. 92 (2012) 283–296.
[54] W. Betz, et al., Bayesian inference with subset simulation: strategies and improvements, Comput. Methods Appl. Mech. Eng. 331 (2018) 72–93.
[55] J. Barros, et al., Adaptive approximate Bayesian computation by subset simulation for structural model calibration, Comput. Aided Civ. Infrastruct. Eng. 37 (6) (2022) 726–745.
[56] M.K. Vakilzadeh, et al., Approximate Bayesian Computation by Subset Simulation using hierarchical state-space models, Mech. Syst. Signal. Process 84 (2017) 2–20.
[57] Z. Feng, et al., Probabilistic updating of structural models for damage assessment using approximate bayesian computation, Sensors 20 (11) (2020) 3197.